PAPER

NJC
www.rsc.org/njc

Lanthanide luminescent mesomorphic complexes with macrocycles derived from diaza-18-crown-6†‡

Stéphane Suárez,[a] Olimpia Mamula,[a] Rosario Scopelliti,[a] Bertrand Donnio,[b] Daniel Guillon,[b] Emmanuel Terazzi,[c] Claude Piguet[c] and Jean-Claude G. Bünzli*[a]

[a] *École Polytechnique Fédérale de Lausanne (EPFL), Laboratory of Lanthanide Supramolecular Chemistry, BCH 1402, CH-1015 Lausanne, Switzerland. E-mail: jean-claude.bunzli@epfl.ch*

[b] *Institut de Physique et Chimie des Matériaux de Strasbourg, Groupe des Matériaux Organiques, UMR 7504, CNRS-Université Louis Pasteur, BP 43, 23, rue du Loess, F-67034 Strasbourg Cedex 2, France*

[c] *Department of Inorganic, Analytical and Applied Chemistry, University of Geneva, 30 quai E. Ansermet, CH-1211 Geneva 4, Switzerland*

Received (in Montpellier, France) 10th March 2005, Accepted 12th July 2005
First published as an Advance Article on the web 29th July 2005

Four tetracatenar (**L1–L4**) and one hexacatenar (**L5**) ligands, derived from the diaza-18-crown-6 framework, are synthesized and characterized. In these ligands, the amine functions are fitted with benzoyloxybenzyl linker groups, attached either with a carbonyl function (**L1**) or a methylene bridge (**L2–L5**) and bearing alkoxy chains, R, of various lengths: R = OCH_3 for **L2**, $OC_{10}H_{21}$ for **L3** and **L5**, $OC_{12}H_{25}$ for **L1**, and $OC_{16}H_{33}$ for **L4**. The non-mesomorphic ligands **L1** and **L3–L5** react with various lanthanide salts to give complexes forming thermotropic hexagonal columnar phases, as ascertained by thermal, optical and small-angle X-ray diffraction methods. The length of the alkoxy chains (**L3** and **L4**) does not much influence the mesogenic behaviour, irrespective of the linker function, the number of alkoxy chains, the counterion or the lanthanide ion. The best systems proved to be the nitrato lanthanide complexes with **L3**, which present a Col_h phase over 100 °C (up to 147 °C for La) with melting transition temperatures between 58 (La) and 86 (Tb) °C. In the case of [$Eu(NO_3)_3$**L3**], chosen as a representative example of all the complexes in this analysis, the inter-column separation of 29.2 Å agrees well with the packing of cylindrical columns resulting from an alternated stacking of the molecules, in which the two mesogenic arms extend on the same side, *i.e.* stacking the molecules in a bent conformation. The liquid crystalline phases containing Eu and Tb display metal-centred emission, meaning that these complexes are interesting building blocks for the design of luminescent liquid crystalline materials.

Introduction

The present upsurge in the design and study of lanthanide-containing mesophases[1] is justified by several potential applications pertaining both to bio-analysis and materials science. For instance, liquid crystal systems are routinely used in protein structure determination by NMR spectroscopy.[2] Since lanthanide-induced shifts are of great help in this respect, combining both the orientation effect of a liquid crystalline phase and the large magnetic anisotropy of, for instance, Yb^{III}, yields an efficient structural method.[3] In addition, lanthanide-containing trichromatic materials emit narrow bands at primary colour wavelengths, and so are employed in lighting devices and displays.[4] Finally, the large magnetic anisotropy of some Ln^{III} ions could also be used to perform magnetic rather than electric switching in liquid crystalline materials.[1,5]

Lanthanide-containing mesophases have largely remained scientific curiosities until the mid 1980s,[6,7] when systematic efforts aimed at isolating lanthanide complexes with liquid crystalline properties started to develop.[8–12] Basically, such materials can be obtained either by mixing lanthanide salts[13] and complexes[14] with mesogenic materials, or by synthesizing lanthanide complexes with mesomorphic properties.

Currently known lanthanide-containing molecular compounds that exhibit liquid crystalline phases belong to four different classes. (i) Lanthanide alkanoates, which form thermotropic smectic A-phases for alkoxy chains bearing between five and fifteen carbon atoms;[15] mesophases can also be induced by doping a non-mesogenic lanthanide dodecanoate with a few percent of the corresponding mesomorphic lanthanide salt.[16] (ii) Schiff base derivatives, which form metallomesogens and several series of mesomorphic lanthanide-containing complexes have been reported since 1991.[8] In particular, reaction of a hydroxybenzaldimine derivative with lanthanide nitrates yields smectic liquid crystals of unusually high magnetic anisotropy.[9,17,18] Recently, mixed 4f–3d columnar metallomesogens have been obtained by adduct formation between a mesomorphic M(salen) complex (salen = 2,2′,*N*,*N*′-bis(salicylidene)ethylenediamine) and a lanthanide nitrate.[19,20] (iii) A third class of compounds takes advantage of tridentate aromatic receptors derived from substituted 2,6-bis(benzimidazolpyridine).[17] A rich variety of mesophases have been reported, for which the type of mesomorphism (calamitic, columnar or cubic) can be tuned by the size of the lanthanide

† Electronic supplementary information (ESI) available: Selected NMR and electronic absorption data, SAXS patterns, luminescence spectra of La and Eu complexes and thermogravimetric analysis of Eu**L3**, see http://dx.doi.org/10.1039/b503591k.

‡ Dedicated to Professor Ernö Brücher on the occasion of his 70th birthday.

DOI: 10.1039/b503591k

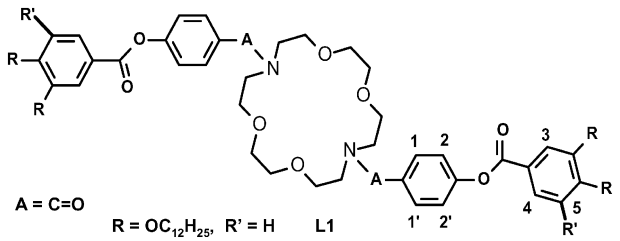

Scheme 1

ion.[21] (iv) Macrocyclic complexes were among the first reported lanthanide-containing mesogens.[7,22,23] They often display discotic phases and most of the receptors used are either phthalocyanines,[7,24,25] benzoporphyrins[26,27] or porphyrins.[28,29] In the former compounds, the lanthanide ion is sandwiched between two macrocycles, and it has been foreseen that these complexes could act as one-dimensional molecular semiconductors.[22] They indeed form hexagonal columnar phases, some of which have been shown to be p-type semiconductors.[27]

To our knowledge, only one paper has reported on the thermal behaviour of lanthanide complexes with a coronand, namely a benzo-15-crown-5 ether derivatised with a 4′-(cholesteryloxy)carbonyl pendant arm. The ligand itself is liquid crystalline, displaying a monotropic chiral nematic mesophase, and its complexes with lanthanide nitrates form highly viscous mesophases.[30] Several substituted diaza crown ethers and their complexes with alkali metal ions are known to be mesomorphic.[31,32] Since diaza crowns form stable complexes with trivalent lanthanide ions,[33] we have investigated whether or not suitably derivatised macrocycles of this type (Scheme 1) are adequate receptors for generating lanthanide complexes that exhibit thermotropic columnar mesomorphism. In a preliminary communication, we have shown that the non-mesomorphic ligand **L3** (Scheme 1) indeed reacts with Eu and Tb nitrates to form luminescent 1 : 1 complexes that display thermotropic columnar hexagonal mesophases over a wide temperature range.[34] Moreover, we have demonstrated that the intensity and lifetime of the Eu- and Tb-centred luminescence can be used to monitor the crystal (Cr) to hexagonal columnar (Col_h) phase transition and *vice versa*.[34,35] In this paper we present the synthesis and characterization of ligands **L1–L5** and their complexes with lanthanide nitrates, triflates and chlorides. The photophysical properties of the complexes are reported and the mesophases obtained are identified from a combination of experimental techniques (thermal analysis, polarized light microscopy and small angle X-ray scattering). We also investigate the parameters influencing the transition temperature, namely the nature of the counterion and the number and length of the alkoxy chains grafted onto the terminal benzyl rings.

Results and discussion

Ligand synthesis

The macrocyclic receptors are built from three different synthons: (i) a 1,10-diaza-4,7,13,16-tetraoxacyclooctadecane core for Ln^{III} complexation—the so-called (2,2) macrocycle, (ii) two anisometric spacers connected to the amine functionalities which also play the role of antennae for sensitizing the Ln^{III} luminescence, and (iii) long terminal alkoxy chains of 10, 12 or 16 carbon atoms connected to the mesogenic spacers. The underlying synthetic principle is a multi-step synthesis of the entire substituent, spacer and alkoxy chain, in the form of a bromide or carboxyl, before coupling them with the (2,2) macrocycle. We have tested two types of spacers, 4-carboxyphenyl benzoate (**L1**) and 4-methylenephenyl benzoate (**L2–L5**). The linking of carboxyl groups confer some rigidity to the ligand, which could be favourable for intermolecular interactions. On the other hand, they also reduce the electron density on the nitrogen atoms, which is detrimental to the complexation of the lanthanide ion, and hence in **L2–L5** have been replaced by methylene bridges. The dicatenar pendant arms of ligands **L1–L4** were synthesized from 3,4-dihydroxybenzoic acid (**1**, Scheme 2) according to the procedure described by Goodby *et al.*[36] A similar strategy was adopted for the synthesis of the tricatenar pendant arm, which was isolated with an overall yield of 38% (Scheme 3). The target ligands were obtained by nucleophilic substitution of the (2,2) macrocycle in a basic medium, with yields of 41, 86, 89 and 42% for **L2**, **L3**, **L4** and **L5** respectively. In the case of **L1**, the corresponding chloride of acid **18** was used as an intermediate in the macrocycle functionalisation (yield 70%).

Single crystals of **L2** suitable for X-ray analysis§ were grown from a mixture of acetonitrile and dichloromethane. They crystallize in the triclinic space group $P\bar{1}$ and their molecular structure, along with the atom numbering scheme, is shown in Fig. 1. The core macrocycle adopts a flat conformation, with an inversion centre located in the middle of the ring. The benzene rings connected to the amine functions are perpendicular to the mean plane of the macrocycle and to the other benzene rings of the arms. The latter extend along the molecular axis, the distance between the furthermost carbon atoms C21 and C21A amounting to 34.15 Å. Overall, the molecule adopts an extended chair conformation. There are two weak intramolecular hydrogen bonds between H1 and O2A (and between H1A and O2), the contact C···O distance being 3.05 Å and the CH···O angle 134.5°. In the crystal packing (Fig. 1), one ligand molecule inserts itself between pairs of molecules lying exactly parallel to each other. The first molecule is linked to the others by a weak intermolecular hydrogen bond between the benzyl H7 atom and the aromatic ring (C8 to C13) of a neighbouring molecule; the contact distance amounts to 2.70 Å and the CH···O angle to 150°.

Interaction of the ligands with lanthanide ions

We have probed the interaction between **L3** or **L4** and lanthanum nitrate by ^{1}H NMR spectroscopy. The ligands in 10^{-2} M deuterated THF have been titrated at room temperature with partially dehydrated $La(NO_3)_3 \cdot xH_2O$ ($x = 3$) and a total of 16 spectra recorded, with ratios $R = [La]_{tot}/[L]_{tot}$ ranging between 0 and 4. The benzyl N-CH_2-Ph and methylene protons from the (2,2) core appear in the range 2.5–4.5 ppm. There is a considerable overlap between the signals of the free and complexed ligand, meaning that only the aromatic region of the spectra yield useful information. Typical spectra for **L3** are shown in Fig. 2. As expected, protons $H^{1,1\prime}$ and $H^{2,2\prime}$ are the most sensitive to complexation, with chemical shift differences between free and bound ligand of about 0.1 ppm (the exact structural assignment of the resonances $H^{1,1\prime}$ and $H^{2,2\prime}$ has not been completed). Two conclusions may be drawn from these spectra. Firstly, only one complexed species is formed, and secondly, the free and complexed ligand are in slow exchange with each other, as observed previously for the corresponding

§ $C_{44}H_{54}N_2O_{12}$, $M = 802.89$, triclinic, $a = 8.7954(11)$, $b = 9.5631(13)$, $c = 13.9798(18)$ Å, $\alpha = 95.811(11)$, $\beta = 91.078(11)$, $\gamma = 115.790(13)°$, $U = 1050.7(2)$ Å^3, $T = 140$ K, space group $P\bar{1}$ (no. 2), $Z = 1$, μ(Mo-Kα) = 0.092 mm^{-1}, 6249 reflections measured, 3242 unique ($R_{int} = 0.0340$) which were used in all calculations. The final wR_2 was 0.1194 (all data). CCDC 276955. See http://dx.doi.org/10.1039/b503591k for crystallographic data in CIF or other electronic format.

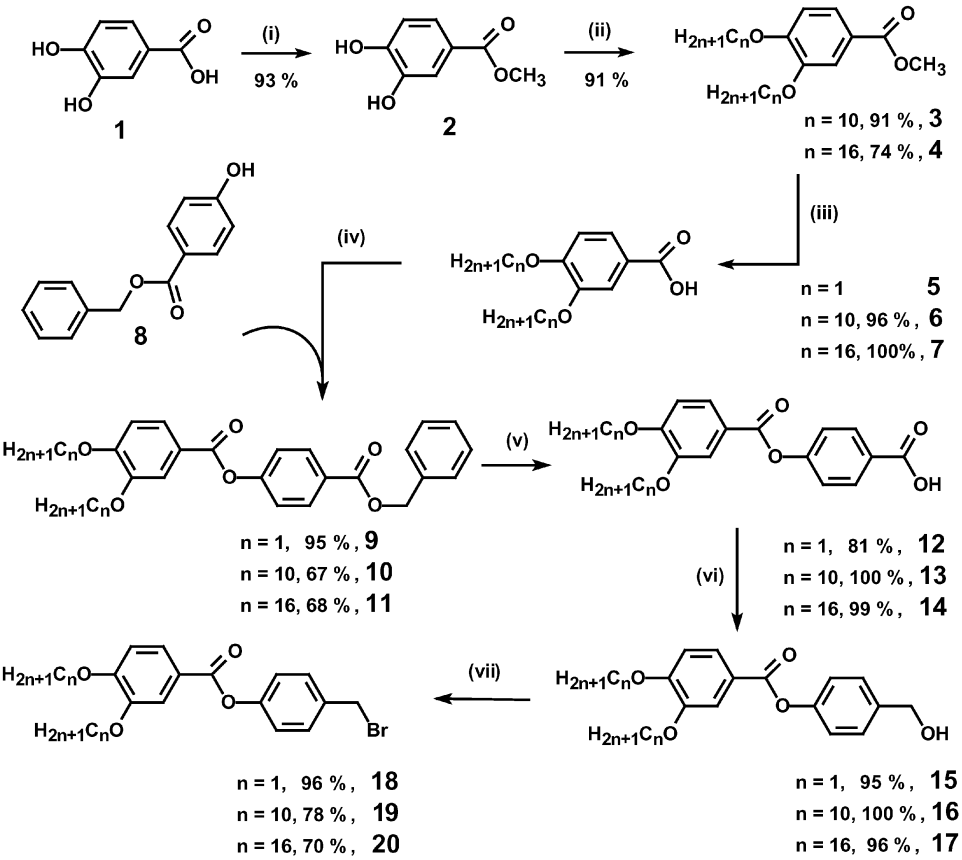

Scheme 2 (i) H_2SO_4, MeOH; (ii) $C_nH_{2n+1}Br$, Cs_2CO_3, butanone; (iii) KOH, EtOH/H_2O; (iv) DCC, DMAP, CH_2Cl_2; (v) Pd/C, THF (for R = benzyl); anisole, CF_3COOH, CH_2Cl_2 (for R = *tert*-butyl); (vi) B_2H_6, THF; (vii) PBr_3, CH_2Cl_2.

complexes of 18-crown-6 ether (18C6).[37] Analysis of the integrated intensity of $H^{1,1\prime}$ and $H^{2,2\prime}$ (Figure S1 and Table S1, ESI†) clearly shows only the formation of 1 : 1 complexes, in line with former studies of lanthanide complexes with 18-membered macrocycles.[33,38] This demonstrates that sandwich complexes of 18C6 ethers form solely in the presence of weakly coordinating anions.[39] From these data, the following stability constants could be extracted: log $K = 2.8 \pm 0.2$ and 2.7 ± 0.2 for ligands **L3** and **L4** respectively.

$$La(NO_3)_3 \cdot 3H_2O\,(solv) + L(solv) \rightleftharpoons [La(NO_3)_3L] + 3H_2O + solv$$

$$K = [La(NO_3)_3L]/[La^{3+}][L]$$

These values are surprisingly low compared to literature data on similar macrocyclic complexes. For instance, a value of log $K = 4.3$ has been determined by NMR spectroscopy for $[La(NO_3)_3(18C6)]$ in acetonitrile, and it is known that replacement of two ether functions by two amine moieties to yield macrocycle (2,2) results in an enhancement of K by 5–6 orders of magnitude in propylene carbonate and in the absence of a coordinating anion.[33] The weak interaction between lanthanum nitrate and the macrocyclic receptors **L3** and **L4** can be traced back to the bulky substituents on the nitrogen atoms, which hinder the necessary flexibility of the ligand to adjust itself to the size of the lanthanide ion, and also which impose unfavourable orientations on the nitrogen lone pairs. Nevertheless, these data unambiguously demonstrate the formation of 1 : 1 nitrato complexes, and that the length of the alkoxy chain has only a marginal effect on the complexation process.

Complexes with the formulae $Ln(NO_3)_3$**L3**$\cdot$solv could be isolated for La (solv = $2H_2O$), Nd (solv = 3 THF), Eu (solv = $0.25H_2O$) and Tb (solv = H_2O), while similar compounds were obtained with **L4** for La (solv = $2H_2O$), Nd (solv = $0.5H_2O$) and Eu (solv = $1.5H_2O$). In addition, 1 : 1 complexes between $Ln(CF_3SO_3)_3$ and **L1** (Ln = La, Eu), $Eu(CF_3SO_3)_3$ and **L3**, $EuCl_3$ and **L3**, $Ln(NO_3)_3$ and **L2** (Ln = La, Eu), and Eu $(CF_3SO_3)_3$ and **L5** were also isolated. Elemental analyses are reported in Table 1. No single crystal amenable to X-ray analysis could be obtained, but a high resolution luminescence

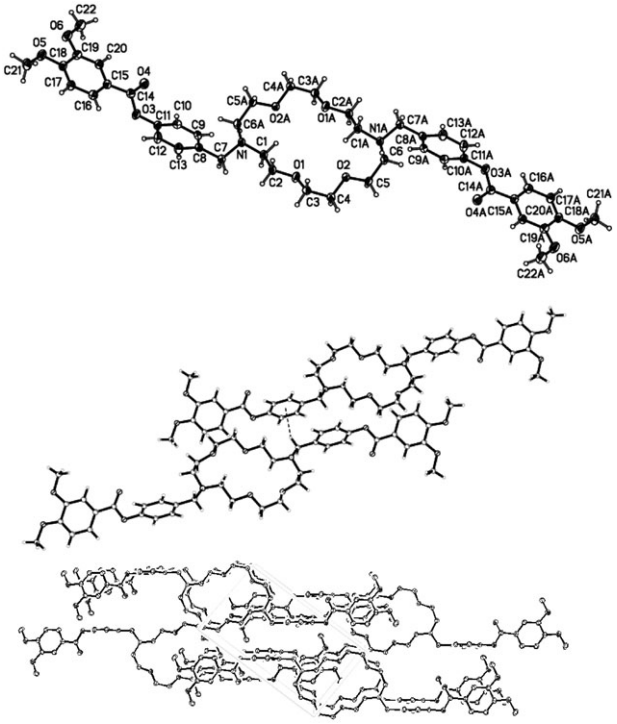

Fig. 1 Molecular structure of **L2** with ellipsoids drawn to 50% probability (top), the unit cell with the H···aryl hydrogen bond evident (middle) and crystal packing (bottom).

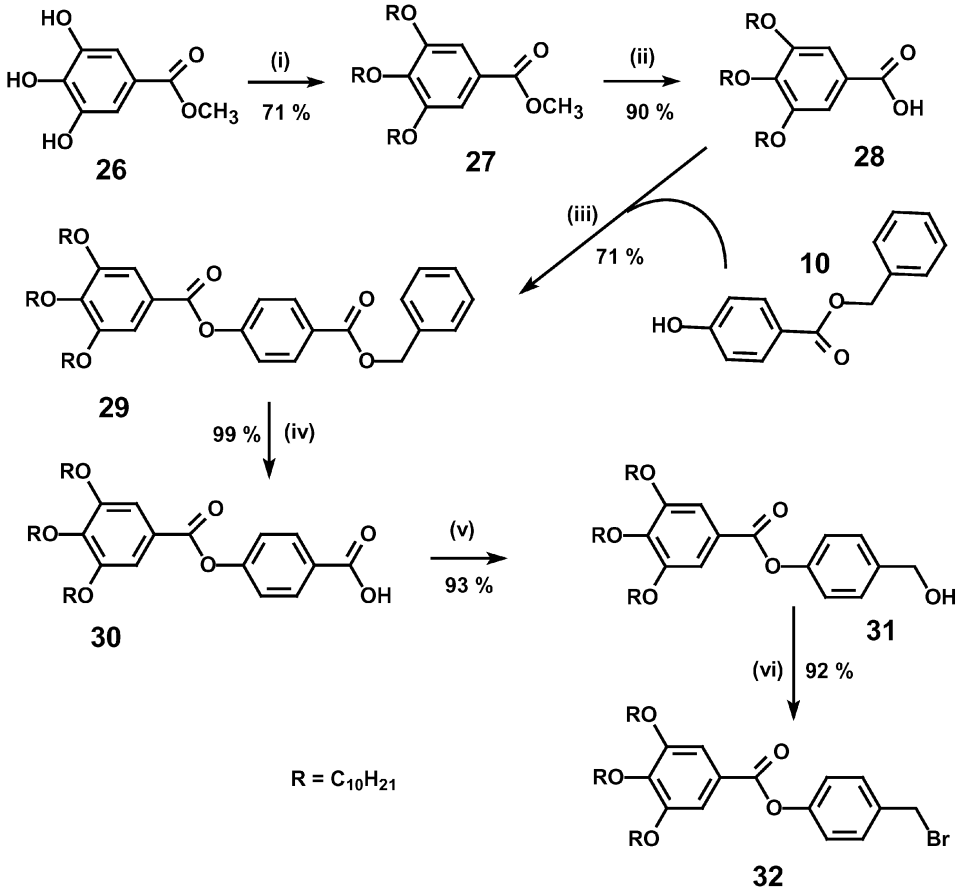

Scheme 3 (i) $C_{10}H_{21}Br$, Cs_2CO_3, butanone; (ii) KOH, EtOH, H_2O; (iii) DCC, DMAP, CH_2Cl_2; (iv) H_2, Pd/C, THF; (v) B_2H_6, THF; (vi) PBr_3 CH_2Cl_2.

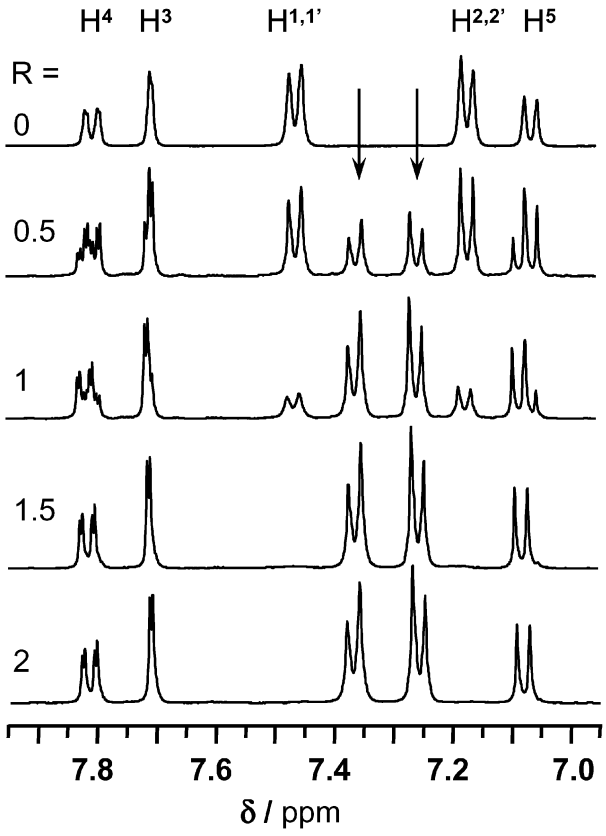

Fig. 2 Aromatic region of the NMR spectrum of 10^{-2} M **L3** in deuterated THF at 298 K, *vs.* the amount of added $La(NO_3)_3 \cdot 3H_2O$; $R = [\mathbf{L3}]_t/[La]_t$; arrows point to resonances specific to the 1 : 1 complex.

study has shown that $Eu(NO_3)_3\mathbf{L3} \cdot 0.25H_2O$ is comprised of two different species in a 3 : 1 proportion; the more abundant being anhydrous and the other featuring one water molecule in the inner coordination sphere of the metal ion.[35,40]

Photophysical properties

Absorption spectra of the ligands (Table 2; Figure S2, ESI†) feature three $\pi \rightarrow \pi^*$ bands around 45 000, 37 000 and 34 000 (with an additional shoulder around 32 500) cm^{-1}. When the length of the alkoxy chain is increased, in going from **L1** to **L3** and **L4**, all the bands sustain a small bathochromic shift, while the addition of two extra alkoxy chains in **L5** results in a larger modification of the spectrum, with the low energy band decreasing in energy and only seen as a shoulder on the broader and substantially red-shifted middle band. It is noteworthy that the presence of carbonyl functions in **L1** does not influence the energy of the electronic absorption bands compared to **L3**. Low temperature luminescence spectra of solid samples under UV excitation allowed us to identify both an emitting singlet state in the spectral range 29 340–30 670 cm^{-1} (26 000 cm^{-1} for **L5**), except for **L2**, and an emitting triplet state in the range 19 590–20 880 cm^{-1}. Emission from the $^1\pi\pi^*$ state disappears as soon as a time delay (0.05 ms) is enforced, confirming the assignment of the two emission bands. The carbonyl groups in **L1** induce a $^1\pi\pi^*$ state 1300 cm^{-1} lower in energy compared to **L3** and **L4**, while the energy of the $^3\pi\pi^*$ state is lowered by about 1000–1290 cm^{-1} with respect to **L2–L5**. The energy difference between the singlet and triplet states, which is of importance in populating the $^3\pi\pi^*$ state through intersystem crossing (ISC), is around 10 000 cm^{-1} for **L1–L4** and 6000 cm^{-1} for **L5**, way above the "ideal" value of 5000 cm^{-1}.[41] Therefore, we do not expect a particularly large sensitization of the metal-centred luminescence.[42]

Table 1 Elemental analyses of the isolated complexes. Calculated values are given within parentheses

Complex	Formula	*fw*	%C	%H	%N
$La(CF_3SO_3)_3$**L1**$\cdot 7H_2O$	$C_{91}H_{138}LaF_9N_2O_{23}S_3 \cdot 7H_2O$	2160.27	50.5 (50.6)	7.1 (7.2)	1.3 (1.2)
$Eu(CF_3SO_3)_3$**L1**$\cdot 3.5H_2O$	$C_{91}H_{138}LaF_9N_2O_{23}S_3 \cdot 3.5H_2O$	2110.27	51.8 (51.6)	6.9 (7.0)	1.3 (1.2)
$La(NO_3)_3$**L2**$\cdot H_2O$	$C_{44}H_{54}LaN_5O_{21} \cdot H_2O$	1145.85	46.1 (46.1)	4.9 (4.9)	6.0 (6.1)
$Eu(NO_3)_3$**L2**$\cdot 1.5H_2O$	$C_{44}H_{54}EuN_5O_{21} \cdot 1.5H_2O$	1153.86	45.4 (44.8)	5.0 (5.0)	5.8 (6.1)
$La(NO_3)_3$**L3**$\cdot 2H_2O$	$C_{80}H_{126}LaN_5O_{21} \cdot 2H_2O$	1668.84	57.6 (57.6)	7.5 (7.9)	4.3 (4.2)
$Nd(NO_3)_3$**L3**$\cdot$ 3THF	$C_{80}H_{126}NdN_5O_{21} \cdot$ 3THF	1854.46	60.1 (59.6)	8.0 (8.2)	3.9 (3.8)
$Eu(NO_3)_3$**L3**$\cdot 0.25H_2O$	$C_{80}H_{126}EuN_5O_{21} \cdot 0.25H_2O$	1650.37	58.0 (58.2)	7.6 (7.7)	4.2 (4.2)
$Eu(CF_3SO_3)_3$**L3**$\cdot$ 0.5THF	$C_{83}H_{126}EuF_9N_2O_{21}S_3 \cdot 0.5$ THF	1943.12	52.4 (52.5)	6.9 (6.7)	1.4 (1.4)
$EuCl_3$**L3**$\cdot$ 2THF	$C_{80}H_{126}Cl_3EuN_2O_{12} \cdot 2$ THF	1710.41	62.2 (61.8)	8.6 (8.4)	1.8 (1.6)
$Tb(NO_3)_3$**L3**$\cdot H_2O$	$C_{80}H_{126}TbN_5O_{21} \cdot H_2O$	1670.84	57.4 (57.5)	7.7 (7.7)	4.1 (4.2)
$La(NO_3)_3$**L3**$\cdot 2H_2O$	$C_{104}H_{174}LaN_5O_{21} \cdot 2H_2O$	2005.48	62.2 (62.3)	8.8 (8.9)	3.6 (3.5)
$Nd(NO_3)_3$**L4**$\cdot 0.5H_2O$	$C_{104}H_{174}NdN_5O_{21} \cdot 0.5H_2O$	1983.8	63.1 (63.0)	9.0 (8.9)	3.4 (3.5)
$Eu(NO_3)_3$**L4**$\cdot 1.5H_2O$	$C_{104}H_{174}EuN_5O_{21} \cdot 1.5H_2O$	2000.53	62.1 (62.4)	8.9 (8.9)	3.5 (3.5)
$Eu(NO_3)_3$**L5**$\cdot 2H_2O$	$C_{100}H_{166}EuN_5O_{23} \cdot 2H_2O$	1994.42	60.2 (60.2)	8.7 (8.6)	3.4 (3.5)

Luminescence spectra of the complexes have been measured on solid state samples at 77 K upon excitation between 40 000 and 30 000 cm^{-1}. The La and Nd complexes displayed emission from both the $^1\pi\pi^*$ (except $Nd(NO_3)_3$**L4**) and $^3\pi\pi^*$ states (Fig. 3; Figure S2 ESI†), from which the energy of the $^1\pi\pi^*$ and $^3\pi\pi^*$ states of the complexed ligands could be deduced (Table S3, ESI†). Most of the complexes with the luminescent lanthanide ions Eu and Tb also display singlet state emission, except $Eu(NO_3)_3$L (L = **L2** and **L4**) and $Eu(CF_3SO_3)_3$**L3**, reflecting the relatively poor efficiency of the ISC process. On the other hand, triplet state emission is completely quenched by ligand-to-metal energy transfer for all the Eu and Tb complexes, with the exception of $Eu(NO_3)_3$**L5**. Lifetimes of the $^5D_0$(Eu) excited states have been determined. Luminescence decays are bi-exponential and the corresponding lifetimes are reported in Table 3. As for $Eu(NO_3)_3$**L3**,[35] its bi-exponential behaviour can be explained by solvation, which generates metal ion sites both with and without coordinated solvent molecules. In the case of $Eu(NO_3)_3$**L3**, the relative contribution to the luminescence decay is 71 ± 3% for the coordination environment without water; for the other complexes, this proportion varies between 60 and 75%. We note that the lifetimes recorded for the three nitrato complexes with **L2–L4** are very similar, pointing to them having a similar inner-sphere arrangement, and particularly to the coordination of the nitrate ions.[35] When the anion is less coordinating (Cl or CF_3SO_3) the lifetime tends to be longer (except for $Eu(CF_3SO_3)_3$**L4**), indicating a less efficient deactivation process compared to the quenching efficiency of nitrate, while the second lifetime becomes shorter.

Thermal properties of the ligands

Transition temperatures and thermodynamic parameters for the investigated ligands are reported in Table 4. Ligand **L1**, in which the pendant arms are attached to the core macrocycle *via* a carbonyl group, melts at 101 °C into its isotropic liquid, after an initial crystalline-to-crystalline transition at low temperature. Its thermal behaviour parallels that of its analogue with C_{10} alkoxy chains, $\mathbf{L1}^{C10}$, which melts at 104 °C.[32] None of the other ligands (**L3**, **L4** or **L5**), in which the pendant groups are linked to the macrocyclic unit by methylene bridges, display mesomorphic behaviour. The addition of a third alkoxy chain in **L5** leads to a dramatic lowering of the melting point, by 48 °C compared to **L3**. The origin of this effect is mainly entropic, the entropic term in **L5** being significantly higher compared to **L3** (see Table 4). The presence of two supplementary alkyl chains in the case of **L5** demands a better organisation of the solid phase in order to accommodate them, and as a consequence, results in an increase in the entropy of the melting process.[43]

Mesomorphic properties of the complexes

Transition temperatures of the complexes (Table 5) were determined by differential scanning calorimetry (DSC), upon heating during the second heating/cooling cycle (see Experimental section). Indeed, most of the complexes are solvated (see elemental analyses, Table 1) and the solvent molecules are liberated during the first heating, which subsequently slightly modifies the mesomorphic properties. We have checked that subsequent heating/cooling cycles generate the same thermograms. Most of the isolated complexes, except those of **L2**, exhibit a liquid crystalline behaviour, most likely resulting from the rigidifying of the systems upon complexation.[5]

$Eu(NO_3)_3$L3. Since the feasibility of using luminescence parameters to detect the crystalline to liquid crystalline phase transition was demonstrated with this complex,[35] its thermal behaviour was also thoroughly investigated. Two differently-hydrated complexes were obtained, dependant on the drying conditions, with 0.25 or 0.5 H_2O per formula weight. Thermogravimetric analysis (Figure S4, ESI†) shows the loss of water of hydration for the latter (loss of 0.54 weight %) between room temperature and 150 °C and that decomposition takes

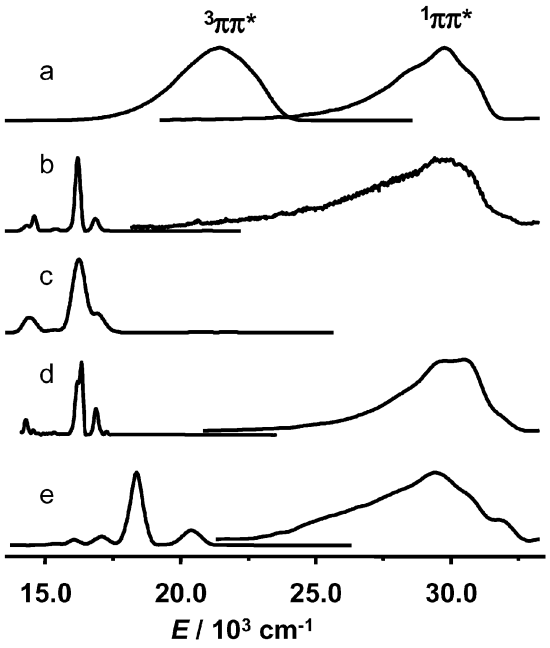

Fig. 3 Emission spectra of the complexes with **L3** at 77 K from solid state samples and under ligand excitation: (a) $La(NO_3)_3$**L3**, (b) $Eu(NO_3)_3$**L3**, (c) $Eu(CF_3SO_3)_3$**L3**, (d) $EuCl_3$**L3**, (e) $Tb(NO_3)_3$**L3**.

Table 2 Photophysical properties of the ligands

Ligand	E/cm^{-1} [a] (log ε)	E/cm^{-1} [b] $^1\pi\pi^*$	E/cm^{-1} [b] $^3\pi\pi^*$
L1	44 840 (4.80) 37 450 (4.54) 33 900 (4.26)	29 340[c]	19 590
L2	45 040 (4.62 sh) 37 590 (4.31) 34 010 (4.05)	[d]	20 620
L3	45 040 (4.71) 37 450 (4.42) 33 900 (4.15)	30 670 29 970 sh	20 760
L4	45 040 (4.76) 37 450 (4.47) 33 900 (4.20)	30 550 29 700 sh	20 660
L5	45 450 (4.82) 36 500 (4.33) 33 780 (4.02 sh)	26 140	20 880

[a] Maximum of the band envelope from absorption spectra in THF, sh = shoulder. [b] From emission spectra of solid state samples at 77 K. [c] At 295 K. [d] Not observed.

Table 3 Lifetimes of the $^5D_0$ excited state (/ms, ±5%) in the Eu complexes upon laser excitation of the $^5D_2$ level

	295 K		77 K	
Complex	τ_1	τ_2	τ_1	τ_2
$Eu(CF_3SO_3)_3$**L1**[a]	[b]	[b]	1.39	0.38
$Eu(NO_3)_3$**L2**	0.78	0.26	1.06	0.38
$Eu(NO_3)_3$**L3**[cd]	0.76	[b]	1.08	0.58
$Eu(NO_3)_3$**L4**	0.78	0.23	1.06	0.40
$EuCl_3$**L3**	1.28	0.33	1.63	0.43
$Eu(CF_3SO_3)_3$**L3**	0.64	0.22	0.95	0.37

[a] Excitation of the $^5D_0$ level (17 259 cm^{-1}). [b] Not determined. [c] From ref. 35. [d] At 10 K; relative population of the site with the longer lifetime 71 ± 3%.

place slightly above 200 °C. Elemental analysis of the former compound (0.25 H_2O) is reported in Table 1, since this compound was used for all the other physicochemical characterizations. During the first heating, the DSC trace (Fig. 4) shows (i) an endothermic feature at 86 °C ($\Delta H = 20$ kJ mol^{-1}, $\Delta S = 56$ J mol^{-1} K^{-1}), corresponding to a transition to a liquid crystalline phase, (ii) an intricate series of exothermic events in the range 125–140 °C, and (iii) endothermic isotropisation, followed by decomposition at around 200–205 °C. The exothermic events occurring at lower temperatures are puzzling since the product is pure. If care is exercised not to heat the compound above 180 °C to avoid any decomposition, they disappear in the subsequent heating/cooling cycles, which can be performed more than ten times without altering the sample. Polarized light optical microscopy (POM) observations revealed birefringent and fluid domains which merged on further heating into large homogeneous textures. The birefringent textures observed show cylindrical and well developed domains, typical of either orthogonal smectic phases (SmA and SmB) or a hexagonal columnar phase (Col_h).[34] It is noteworthy that no transition was detected between 86 and 200 °C by this technique, except isotropisation. Similar situations have been reported—for instance, in the case of Pd(II) complexes with macrocyclic polycatenar receptors.[44] Finally, we have resorted to small angle X-ray scattering (SAXS) to fully identify the nature of the mesophase. As expected from the DSC traces, a change in the X-ray pattern corresponding to a modification of the molecular packing was detected between 80 and 90 °C. This change was characterized by the disappearance of the intense and sharp peaks of the crystalline phase and the appearance of a small angle reflection with a periodicity of about 45 Å, along with a broad scattering at 4.6 Å, corresponding to the liquid-like ordering of the chains (Fig. 5). The large periodicity is in agreement with the packing of the complex into smectic layers and in agreement with the length of the molecule estimated from molecular models. From the molecular volume, V, estimated to 2800 Å^3, the molecular area is found to be 60 Å^2 for two chains (see Fig. 6(a)), consistent with a smectic phase. This value also suggests that the chains are in a disordered coil conformation so as to compensate for the large molecular area of the central macrocycle, or that they are interdigitated with the chains of the neighbouring layers. On further heating, the X-ray pattern is transformed once more at 150 °C, and remains unchanged up to 200 °C. Fig. 5 presents the diffraction pattern of the latter, which is also evident during subsequent heating/cooling cycles. It features a broad diffuse halo at 4.6 Å and three small angle diffraction peaks (Table S3, ESI†) corresponding to distances of 25.3, 14.5 and 12.5 Å, which are in the relationship $1 : 1/\sqrt{3} : 1/\sqrt{4}$, characteristic of a hexagonal columnar phase, Col_h, with an inter-column separation of 29.2 Å and a cross-section area of $S = 740$ Å^2 (Fig. 6(c)).[45] The diffuse band around 4.6 Å is assigned to the liquid-like order of the molten alkoxy substituents. The absence of additional features in the wide angle part of the diffractogram, apart from this diffuse band, suggests a short range correlation of the molecular stacking within the column. During the cooling process (of the mesophase to ensure the absence of decomposition) the pattern of the Col_h phase persists down to 40 °C without any change in phase structure or spacing distances. Therefore, the thermal event observed during the first heating around 150 °C probably corresponds to the transition of a transient metastable mesophase (lamellar type) into a hexagonal arrangement of the molecules, a likely consequence of a change of macrocyclic conformation, induced perhaps by water loss. By taking a typical stacking period to be approximately $h \approx 4.5$ Å between two stacked complexes within the column (*i.e.* the associated broad peak could be masked by one of the molten chains)[17] and a density of $d = 1$ for the Col_h mesophase, we calculate $Z = (d \times N_{Av} \times V \times 10^{-24})/FW = 1.1(1)$, *i.e.* ≈ 1 molecule per unit cell (N_A is Avogadro's number, FW is the formula weight of the molecule in g mol^{-1} and V is the volume of the unit cell in Å^3).[46] This is consistent with either a single hemi-disk-like complex [$Eu(NO_3)_3$**L3**] occupying the cross-section of one column, or two complex molecules occupying a cell 9 Å thick (Fig. 6). The length of the coordinated ligand strand in its bent form in [$Eu(NO_3)_3$**L3**] can be reasonably estimated from the crystal structures of **L2** (Fig. 1) and [Eu(2,2)$(NO_3)_3$][47] as amounting to $L \approx 29$ Å, in very good agreement with the inter-column separation found in the Col_h mesophase (Fig. 6(a)).[18] Since coordination of the bulky $Ln(NO_3)_3$ metallic unit restricts intermolecular π-stacking between adjacent packed complexes, we propose that the complexes in one column adopt head-to-tail orientations to ensure (i) weak intra-columnar packing *via* the aromatic groups and (ii) pseudo-circular spreading of the flexible chains (Fig. 6(b)).

Other complexes. The results of the thermal and optical analyses performed on the other complexes are summarized in Table 5. The transition temperatures for complexes Eu $(CF_3SO_3)_3$**L1** and $Eu(NO_3)_3$**L5** have been determined by POM only, since no first order transition was observed by DSC. The two compounds are, however, mesomorphic in the range 145–163 °C and 110–135 °C respectively. For Eu $(NO_3)_3$**L5**, the mesophase is not seen during the first heating

Table 4 Thermal properties of the ligands[a]

Compound	Transition	T/°C	ΔH/kJ mol^{-1}	ΔS/J mol^{-1} K^{-1}
L1	Cr–Cr′	42	4	13
	Cr–I	101	95	254
L2	Cr–I	166	99	226
L3	Cr–I	85	100	279
L4	Cr–I	93	120	328
L5	Cr–I	37	94	303

[a] Cr = crystal, I = isotropic liquid.

but is obtained in the first cooling and is present in subsequent heating/cooling cycles. The other complexes display the same behaviour as $Eu(NO_3)_3$**L3**. During the first heating, they sustain a phase transition from either a crystalline or a lamellar mesophase into an isotropic liquid phase, which, upon heating, transforms into a mesophase. The latter remains unchanged during the cooling process and also reappears during the subsequent heating/cooling cycles, provided that the decomposition temperature is not reached. According to SAXS measurements, the luminescent EuX_3**L3** (X = NO_3 and Cl), $Tb(NO_3)_3$**L3** and $Eu(NO_3)_3$**L4** complexes present, in addition to the broad and weak reflection associated with the melting of the aliphatic chains (at ≈ 4.6 Å), three low-angle reflections—their associated distances pointing unambiguously to the presence of a Col_h mesophase, similar to the one characterized by the diffractogram shown in Fig. 5.

Parameters influencing the formation of the liquid crystalline phases in the studied complexes. The structure of the ligand influences considerably the formation of the mesophases, as exemplified by the complexes $Eu(CF_3SO_3)_3L$ with L = **L1** and **L3**. The temperature range in which the latter is liquid crystalline (90–195 °C) is four times larger than is the case for the former, while its mesophase forms at a much lower temperature (145 °C for the complex with **L1**). Replacing the carbonyl bridge in **L1** with a methylene linkage in **L3** results in a lowering of the ligand polarity and an increased flexibility. However, metal coordination rigidifies the systems and so could diminish the differences between them. It is known that the introduction of nitrogen atoms into crown ethers is favourable for the coordination by lanthanide ions.[42] Here however, the nucleophilicity of the amine functionality is considerably reduced by the presence of the carbonyl groups in **L1**, which may result in some dissociation of the complex and thus in a shrinkage of the mesophase domain by the presence of solid free lanthanide salt and/or liquid ligand (fusion at 101 °C).

Table 5 Transition temperatures in some of the studied complexes with associated thermodynamic parameters (±1 °C), as determined by DSC (second heating)

Complex	Transition[a]	T/°C	ΔH/kJ mol^{-1}	ΔS/J mol^{-1} K^{-1}
$La(NO_3)_3$**L3**	Cr–Col_h	58	13	40
	Col_h–I[b]	205	81	171
$Nd(NO_3)_3$**L3**[b]	Cr–Col_h	85	25	71
$Eu(NO_3)_3$**L3**[b]	Cr–Col_h	86	20	56
$Tb(NO_3)_3$**L3**[b]	Cr–Col_h	81	11	32
$EuCl_3$**L3**[b]	Cr–Col_h	75	32	92
$La(NO_3)_3$**L4**	Cr–Col_h	71	23	67
	Col_h–I	199	48	101
$Nd(NO_3)_3$**L4**[b]	Cr–Col_h	88	36	100
$Eu(NO_3)_3$**L4**	Cr-Col_h	84	13	35

[a] Cr = crystal, semi-crystal or amorphous, I = isotropic liquid, Col_h = hexagonal columnar. [b] Decomposition occurs shortly after isotropisation meaning that the transition temperature (and whenever relevant, the associated thermodynamic parameters) could only be determined reliably during the first heating cycle (see Fig. 7).

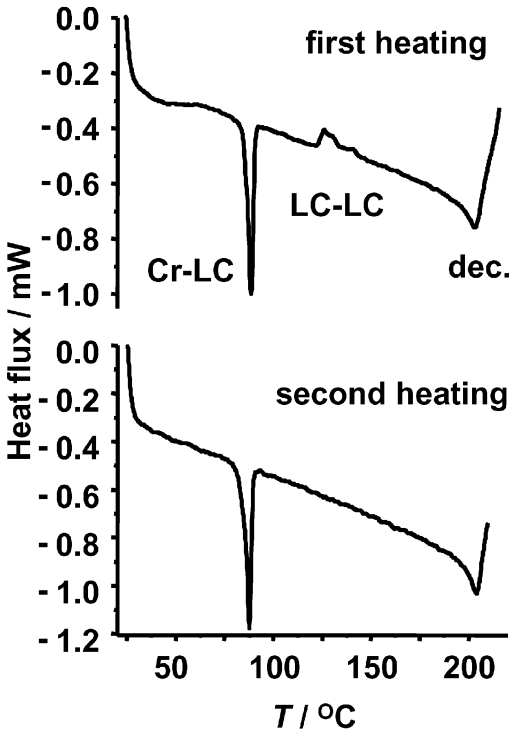

Fig. 4 DSC traces of the [$Eu(NO_3)_3$**L3**] complex during the first (top) and second (bottom) heating cycle, after the first heating cycle did not reach sample decomposition temperature (5 °C min^{-1}, under N_2 atmosphere).

As far as the counterion is concerned, the nitrato complexes possess the best mesomorphic properties, as demonstrated by the series of complexes EuX_3**L3** (X = NO_3, Cl and CF_3SO_3). The influence of the metal ion on the temperature range of the Col_h mesophase in nitrato complexes is illustrated in Fig. 7, as determined by calorimetry and polarized light microscopy. While all the complexes studied present the same Col_h mesophase, its temperature range depends heavily on the nature of the metal ion. La leads to the largest range (147 °C) and lowest transition temperature (58 °C), while the luminescent complexes of Eu and Tb have higher transition temperatures (≈85 °C) but remain liquid crystalline up to almost 200 °C. The length of the alkoxy chain does not seem to play an essential role, since data for complexes with **L3** (C_{10}) and **L4** (C_{16}) are almost identical. The exception here is La, the temperature range of the mesophase here being reduced by about 20 °C in its **L4** complex. Finally, we have investigated the influence of the number of alkoxy chains by designing the hexacatenar ligand, **L5**. The addition of two more flexible alkoxy chains to **L3** to

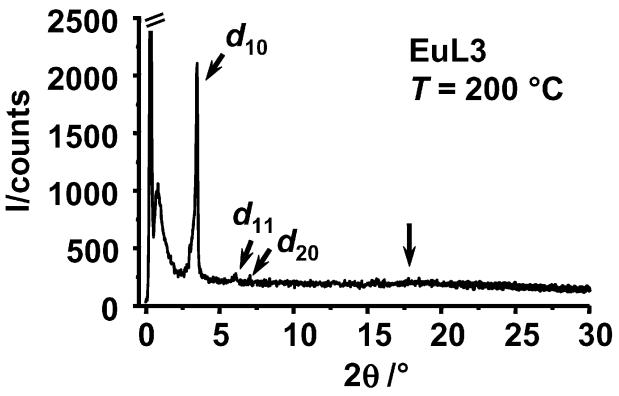

Fig. 5 SAXS diffractogram of [$Eu(NO_3)_3$**L3**] during the first heating at 200 °C, displaying the characteristic pattern of a columnar hexagonal phase.

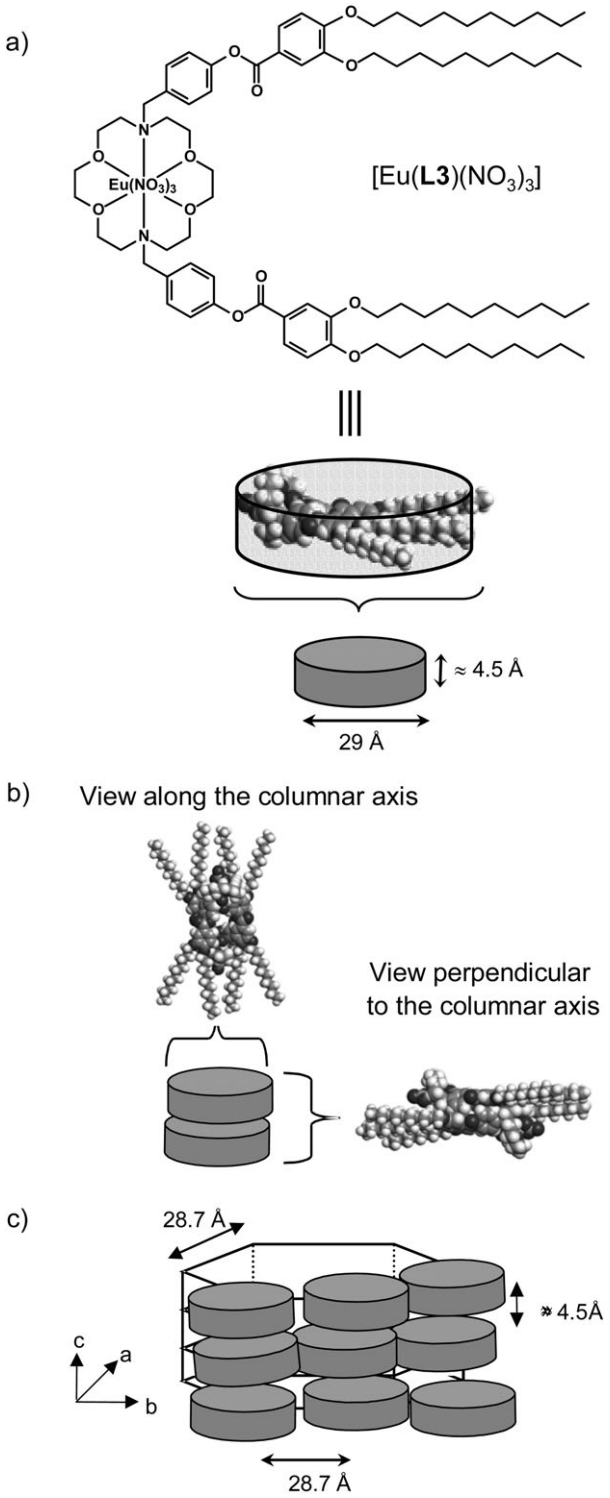

Fig. 6 Molecular modelling of [Eu(NO$_3$)$_3$**L3**] in the Col$_h$ mesophase (see text). Schematic representations of (a) the unit cell, (b) the head-to-tail packing of two adjacent cells within a column and (c) the arrangement of the columns within the hexagonal lattice.

yield **L5** leads both to an increase (24 °C) in the temperature at which the mesophase appears (110 °C for Eu(NO$_3$)$_3$**L5**) and a large decrease (70 °C) in the isotropisation temperature, resulting in a very narrow mesomorphic range (25 °C as compared to 114 °C for the complex with tetracatenar **L3**).

Conclusion

Complexation of lanthanide salts to the derivatised (2,2) macrocyclic ligands **L1** and **L3–L5** rigidifies the receptor framework and confers an increased polarity on the resulting

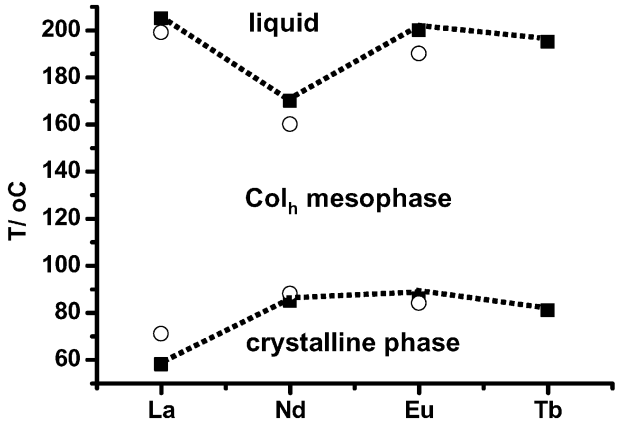

Fig. 7 Phase diagram for the complexes Ln(NO$_3$)$_3$L (■: L = **L3**, Ln = La, Nd, Eu and Tb; ○: L = **L4**, Ln = La, Nd and Eu).

complexes. This in turn leads to intermolecular interactions strong enough to form hexagonal columnar mesophases, while the ligands themselves, with the exception of **L1**, are non-mesomorphic. The more stable mesophases occur with lanthanide nitrates and the tetracatenar ligands **L3** and **L4**, which feature a methylene moiety in the spacer between the macrocyclic core and the pendant mesogenic groups. Indeed the presence of a carbonyl function in the linking unit of **L1** reduces the complexation ability of the ligand and yields less thermally-stable complexes and mesophases. Of those ligands examined, the best proved to be **L3**, which bears four decyloxy chains, since the corresponding complexes exhibit a Col$_h$ mesophase. The latter starts to form between 58 and 86 °C and often extends over a 100 °C temperature range, up to 147 °C for La. The liquid crystalline phases containing luminescent Ln ions (Eu and Tb) retain their emission properties almost up to isotropization.[35] Therefore, these systems could represent interesting building blocks for the design of liquid crystalline luminescent materials, providing the transition temperature is lowered and the antenna effect is optimized. Work toward this goal is currently in progress in our laboratory.

Experimental

Sample handling

The mesomorphic complexes display a decomposition temperature close to the isotropisation temperature. As a result, initial physicochemical experiments led to decomposition of the samples. To cope with this problem, samples for DSC, POM, luminescence and SAXS measurements were handled under an inert atmosphere of nitrogen. Moreover, in the case of the DSC and luminescence experiments reported in ref. 35, the samples were not heated too high (to around 180 °C) in order to avoid such problems. As a consequence, transition temperatures were easily reproduced. For instance, the following temperature transitions were obtained for the europium–nitrato complex with **L3** during six heating/cooling cycles: T = 85.5, 86.3, 86.7, 86.6, 85.1 and 85.4 °C. For this particular sample, this transition temperature has also been confirmed by four other independent measurements (polarized light microscopy and small angle X-ray diffraction measured on three different instruments) with temperatures ranging from 83 to 86 °C, depending on the experimental technique. For POM experiments, the samples were only kept for a few seconds at the isotropisation temperature. For SAXS measurements, both techniques were used (heating/cooling cycles with maximum temperatures lower than the isotropisation temperature and leaving the samples for only a few seconds at the latter temperature). In any given case, when quantitative thermo-

dynamic parameters are quoted (*e.g.* Table 5), they are the average of at least three determinations.

Physicochemical measurements

IR spectra were obtained either from KBr pellets on a Mattson α-Centauri FT-IR spectrometer or from powders on a Spectrum One FT-IR Perkin-Elmer instrument fitted with an ATR attachment. Electronic spectra in the UV-vis range were recorded with a Perkin-Elmer Lambda-900 spectrometer in 1.0 and 0.1 cm quartz cells. Semi-empirical calculations were performed with the CAChe Pro 6.1 program package for Windows® (Fujitsu Ltd., 2000–2003). ^{1}H and ^{13}C NMR spectra were recorded at 25 °C on either a Bruker AM-360 (360 MHz) or AVANCE 400-DRX (400 MHz) spectrometer. Mass spectra were obtained at EPFL using a Finnigan SSQ-710C or LCQ deca XP plus spectrometer, or at the University of Fribourg (Switzerland) on a Bruker FTMS 4.7T BioPEX II spectrometer. Low-resolution luminescence spectra were measured on a Perkin-Elmer LS-50B spectrometer. Experimental procedures for lifetime measurements under high resolution selective excitation have been published previously.[48] Bi-exponential luminescence decays were fitted to the equation:

$$I(t) = A_1 e^{-k_1 t} + A_2 e^{-k_2 t} + B, \text{ where } 1/k = \tau$$

where $I(t)$ is the luminescence intensity *versus* time, A_1 and A_2 are pre-exponential parameters, k_1 and k_2 are the de-activation rate constants, and τ is the lifetime of the excited state. DSC thermograms were collected on Setaram DSC-131 S and Seiko DSC-220C instruments at 5–10 °C min^{-1} under a nitrogen atmosphere. Thermogravimetric analyses were performed with a Seiko TG/DTA 320 balance under a nitrogen atmosphere. POM was performed on a Leitz Orthoplan-Pol microscope equipped with a Leitz LL 20 × 0.40 polarization lens, a Linkam THMS 600 variable temperature oven and a Leica D300 F camera.

Synthesis and characterisations

Solvents and starting materials were purchased from Fluka AG (Buchs, Switzerland) and Acros. Acetonitrile and dichloromethane were distilled from CaH_2, THF was distilled over sodium and benzophenone, and triethylamine was distilled from KOH. The following intermediates were commercial compounds: **6** (Aldrich), **10** (Lancaster) and **26** (Acros). Lanthanide trifluoromethanesulfonates (triflates)[49] and nitrates[50] were prepared from the oxides (Rhône-Poulenc, 99.99%) and the corresponding trifluoroacetic or nitric acid. Their metal content was determined by titration with Na_2EDTA-H_2 in the presence of urotropine and xylene orange.[51] Elemental analyses were performed by Dr. H. Eder (Microchemical Laboratory), University of Geneva, Switzerland.

Methyl 3,4-di(hydroxyl)benzoate (**2**)[52] and 4-hydroxybenzoic acid *tert*-butylester (**11**) were prepared as reported in the literature.[53] Methyl 3,4-di(decyloxy)benzoate (**3**, yield 91%), methyl 3,4-di(dodecyloxy)benzoate (**4**, 89%), methyl 3,4-di(hexadecyloxy)benzoate (**5**, 74%), 3,4-di(decyloxy)benzoic acid (**7**, 96%), 3,4-di(dodecyloxy)benzoic acid (**8**, 85%), 3,4-di(hexadecyloxy)benzoic acid (**9**, 100%), 4-[3,4-di(decyloxy)benzoyloxy] benzoate (**13**, 67%), 4-[3,4-di(hexadecyloxy)benzoyloxy] benzoate (**14**, 68%), 4-[3,4-di(decyloxy)benzoyloxy] benzoic acid (**17**, 100%), and 4-[3,4-di(hexadecyloxy)benzoyloxy] benzoic acid (**19**, 100%) were synthesised according to Goodby *et al.*[36] and characterized by NMR spectroscopy. The similar tricatenar derivatives (see Scheme 3) **27** (71%), **28** (90%), **29** (71%) and **30** (99%) were obtained by following the same protocols. [36] In the synthesis of **28**, due to the formation of an emulsion after the acidification of the reaction, the solvent (ethanol) was evaporated and the residue extracted from a mixture of dichloromethane and dilute HCl. The organic phase was washed with water until a neutral pH was obtained, dried over $MgSO_4$, and after the evaporation of the solvent, **28** recovered as a white powder.

4-[3,4-Di(methoxy)benzoyloxy] benzoate (12). Benzyl 4-hydroxybenzoate **10** (2.51 g, 11 mmol), 4-(*N*,*N*-dimethylamino)pyridine (DMAP; 1.34 g, 11 mmol), *N*,*N*′-dicyclohexylcarbodiimide (DCC; 2.27 g, 11 mmol) and veratric acid (2 g, 11 mmol) were heated under reflux for 48 h in dichloromethane (60 cm^3). The solvent was removed under reduced pressure and the residue purified by flash column chromatography (silica gel, 40–60 μm) using a mixture of $CHCl_3$/methanol (98 : 2) as eluent to give 4.09 g (95%) of **12** as white powder. δ_H (400 MHz, $CDCl_3$, 25 °C, TMS): 8.15 (2 H, d, $^3J = 9$ Hz), 7.85 (1 H, dd, $^3J = 9$, $^4J = 2$ Hz), 7.66 (1 H, d, $^4J = 2$ Hz), 7.3–7.5 (5 H, m), 7.28 (2 H, d, $^3J = 9$ Hz), 6.95 (1 H, d, $^3J = 9$ Hz), 5.38 (2 H, s), 3.97 (3 H, s) and 3.96 (3 H, s).

4-[3,4-Di(dodecyloxy)benzoyloxy] tert-butanoate (15). Following a modified procedure,[54] **8** (8 mmol, 3.92 g), **11** (8 mmol, 1.55 g), DCC (8 mmol, 1.64 g) and DMAP (8 mmol, 0.97 g) were refluxed under an inert atmosphere in dichloromethane (200 cm^3) for 60 h. The warm mixture was filtered and the filtrate obtained absorbed onto a small amount of silica gel, which, after the elimination of the solvent, was placed on the top of a silica gel column (hexane : ethyl acetate, 95 : 5) and purified by chromatography. Yield: 68%. δ_H (400 MHz, $CDCl_3$): 8.07 (2 H, d, $^3J = 8.6$ Hz), 7.81 (1 H, dd, $^3J = 8.6$, $^4J = 2.0$ Hz), 7.66 (1 H, d, $^4J = 2.0$ Hz), 7.25 (2 H, d, $^3J = 8.5$ Hz), 6.94 (1 H, d, $^3J = 8.6$), 4.07 (4 H, m), 1.87 (4 H, m), 1.58 (9 H, s), 1.52–1.43 (6 H, m), 1.40–1.23 (32 H, m) and 0.87 (4 H, m). MS (CI): $m/z = 667$ (M^+, 8%), 473 ($M^+ - C_6H_4COO^tBu$, 100%) and 137 ($M^+ - 2OC_{12}H_{25}$-$C_6H_4COO^tBu$, 33%).

4-[3,4-Di(methoxy)benzoyloxy] benzoic acid (16).[55] Compound **12** (4.08 g, 10.39 mmol) was dissolved in THF (100 cm^3) and 10% of Palladium on charcoal catalyst added (0.43 g). The reaction was stirred under a hydrogen atmosphere for 3 h. The catalyst was removed by filtration through Celite and the solvent removed under reduced pressure to give 2.60 g (81%) of **16**. δ_H (400 MHz, $CDCl_3$, 25 °C, TMS): 7.87 (2 H, d, $^3J = 9$ Hz), 7.61 (1 H, dd, $^3J = 9$, $^4J = 2$ Hz), 7.42 (1 H, d, $^4J = 2$ Hz), 7.04 (2 H, d, $^3J = 9$ Hz), 6.76 (1 H, d, $^3J = 9$ Hz), 3.72 (3 H, s) and 3.71 (3 H, s).

4-[3,4-Di(dodecyloxy)benzoyloxy] benzoic acid (18). Following a modified procedure,[53] a solution of ester **15** (167 mg, 0.25 mmol) in dichloromethane (10 cm^3) was cooled to 0 °C. Anisole (1 cm^3) followed by trifluoroacetic acid (2.5 cm^3) were added and the mixture stirred at 0 °C for 3 h and then 1 h at room temperature. The evaporation of the solvent lead to a neat white precipitate of **18** which was washed with diethyl ether (20 cm^3) and dried. Yield: 82%. δ_H (400 MHz, $CDCl_3$): 8.21 (2 H, d, $^3J = 8.8$ Hz), 7.83 (1 H, dd, $^3J = 8.4$, $^4J = 2.0$ Hz), 7.67 (1 H, d, $^4J = 2.0$ Hz), 7.34 (2 H, d, $^3J = 8.8$ Hz), 6.95 (1 H, d, $^3J = 8.4$ Hz), 4.09 (4 H, m), 1.87 (4 H, m), 1.49 (4 H, m), 1.4–1.2 (32 H, m) and 0.89 (6 H, m). MS (CI): $m/z = 611$ (M^+, 23%), 628 ($M^+ + NH_3$, 74%), 667 ($M^+ + NH_3 + K^+$, 21%), 684 ($M^+ + 2NH_3 + K^+$, 100%), 473 ($M^+ - OC_6H_4COOH$, 60%), 305 ($M^+ - OC_6H_4COOH - C_{12}H_{25}$, 10%) and 137 ($M^+ - OC_6H_4COOH - 2C_{12}H_{25}$, 12%).

4-[3,4-Di(methoxy)benzoyloxy] benzyl alcohol (20). Compound **16** (2.49 g, 8.22 mmol) was dissolved in THF (50 cm^3) and 1 M diborane in THF (12.5 cm^3) was added under an inert atmosphere. The mixture was stirred for 24 h and water (50 cm^3) then added carefully. After removal of THF, the precipitate was washed with further water to give 2.25 g (95%) of

20. δ_H (400 MHz, $CDCl_3$, 25 °C, TMS): 3.46 (3 H, s), 3.49 (3 H, s), 4.20 (2 H, s), 6.64 (1 H, d, $^3J = 8$ Hz), 6.78 (2 H, d, $^3J = 8$ Hz), 7.00 (2 H, d, $^3J = 8$ Hz), 7.23 (1 H, d, $^4J = 2$ Hz) and 7.39 (1 H, dd, $^3J = 8$, $^4J = 2$ Hz).

4-[3,4-Di(decyloxy)benzoyloxy] benzyl alcohol (21). Prepared by a method similar to that described for **20**. Yield: 1.59 g (100%). δ_H (400 MHz, $CDCl_3$, 25 °C, TMS): 0.88 (6 H, m), 1.21–1.53 (28 H, m), 1.84 (4 H, m), 4.06 (4 H, m), 4.72 (2 H, s), 6.92 (1 H, d, $^3J = 9$ Hz), 7.18 (2 H, d, $^3J = 8$ Hz), 7.41 (2 H, d, $^3J = 8$ Hz), 7.66 (1 H, d, $^4J = 2$ Hz) and 7.80 (1 H, dd, $^3J = 9$, $^4J = 2$ Hz).

4-[3,4-Di(hexadecyloxy)benzoyloxy] benzyl alcohol (22). Prepared by a method similar to that described for **15**. Yield: 5.15 g (96%). δ_H (400 MHz, $CDCl_3$, 25 °C, TMS): 7.80 (1 H, dd, $^3J = 9$, $^4J = 2$ Hz), 7.66 (1 H, d, $^4J = 2$ Hz), 7.42 (2 H, d, $^3J = 9$ Hz), 7.19 (2 H, d, $^3J = 9$ Hz), 6.92 (1 H, d, $^3J = 9$ Hz), 4.72 (2 H, d, $^3J = 5$ Hz), 4.07 (4 H, m), 1.84 (4 H, m), 1.53–1.21 (52 H, m) and 0.88 (6 H, m).

4-[3,4-Di(methoxy)benzoyloxy] benzyl bromide (23). Phosphorus tribromide (1.4 cm^3, 14.9 mmol) was added under an inert atmosphere to a solution of **20** (2.15 g, 7.46 mmol) in dry dichloromethane (20 cm^3). The mixture was heated under reflux for 48 h and water (20 cm^3) added carefully. The compound was extracted with dichloromethane (3 × 20 cm^3) and dried over Na_2SO_4. After removal of the solvent, 2.51 g (96%) of **23** were obtained as a white powder. δ_H (400 MHz, $CDCl_3$, 25 °C, TMS): 7.84 (1 H, dd, $^3J = 9$, $^4J = 2$ Hz), 7.66 (1 H, d, $^4J = 2$ Hz), 7.44 (2 H, d, $^3J = 9$ Hz), 7.18 (2 H, d, $^3J = 9$ Hz), 6.95 (1 H, d, $^3J = 9$ Hz), 4.52 (2 H, s), 3.98 (3 H, s) and 3.97 (3 H, s).

4-[3,4-Di(decyloxy)benzoyloxy] benzyl bromide (24). Phosphorus tribromide (2.4 cm^3, 25.5 mmol) was added under an inert atmosphere to a solution of **21** (4.12 g, 7.62 mmol) in dry dichloromethane (60 cm^3). The mixture was heated under reflux for 96 h and water (50 cm^3) added carefully. The compound was extracted with $CHCl_3$ (3 × 70 cm^3) and purified by flash column chromatography (silica gel, 40–60 μm) using dichloromethane as eluent to give 3.61 g (78%) of **24**. δ_H (400 MHz, $CDCl_3$, 25 °C, TMS): 7.78 (1 H, dd, $^3J = 8$, $^4J = 2$ Hz), 7.64 (1 H, d, $^4J = 2$ Hz), 7.43 (2 H, d, $^3J = 9$ Hz), 0.88 (6 H, m), 7.16 (2 H, d, $^3J = 9$ Hz), 6.91 (1 H, d, $^3J = 8$ Hz), 4.52 (2 H, s), 4.06 (4 H, m), 1.85 (4 H, m) and 1.53–1.21 (28 H, m).

4-[3,4-Di(hexadecyloxy)benzoyloxy] benzyl bromide (25). Prepared by a method similar to the one described for **24**. Yield: 3.81 g (70%). δ_H (400 MHz, $CDCl_3$, 25 °C, TMS): 7.79 (1 H, dd, $^3J = 9$, $^4J = 2$ Hz), 7.65 (1 H, d, $^4J = 2$ Hz), 7.44 (2 H, d, $^3J = 9$ Hz), 7.17 (2 H, d, $^3J = 9$ Hz), 6.92 (1 H, d, $^3J = 9$ Hz), 4.52 (2 H, s), 4.06 (4 H, m), 1.85 (4 H, m), 1.53–1.21 (52 H, m) and 0.88 (6 H, m).

4-[3,4,5-Tri(decyloxy)benzoyloxy] benzyl alcohol (31). This compound was prepared by a method similar to that described for **21**. Yield: 93%. δ_H (400 MHz, $CDCl_3$, 25 °C, TMS): 7.43 (2 H, d, $^3J = 8.4$ Hz), 7.41 (2 H, s), 7.19 (2 H, d, $^3J = 8.4$ Hz), 4.74 (2 H, s), 4.05 (6 H, m), 1.87–1.73 (6 H, m), 1.49 (6 H, m), 1.30 (36 H, br) and 0.89 (9 H, m). MS (CI): m/z = 697 (M^+, 92%), 714 ($M^+ + NH_3$, 98%) and 574 ($M^+ - OC_6H_4CH_2OH$, 100%).

4-[3,4,5-Tri(decyloxy)benzoyloxy] benzyl bromide (32). This compound was prepared in the same way as **24**. Yield: 92%. δ_H (400 MHz, $CDCl_3$, 25 °C, TMS): 7.46 (2 H, d, $^3J = 8.3$ Hz), 7.40 (2 H, s), 7.18 (2 H, d, $^3J = 8.3$ Hz), 4.53 (2 H, s), 4.05 (6 H, m), 1.88–1.73 (6 H, m), 1.49 (6 H, m), 1.28 (36 H, br) and 0.89 (9 H, m). MS (CI): m/z = 760 (M^+, 5%) and 574 ($M^+ - OC_6H_4CH_2Br$, 100%).

***N,N′*-bis{4-[3,4-di(decyloxy)benzoyloxy]benzoyl}-1,10-diaza-4,7,13,16-tetraoxacyclooctadecane (L1).** Under an inert atmosphere, a solution of acid **18** (183 mg, 0.3 mmol) in freshly distilled dichloromethane (3 cm^3) was cooled to 0 °C using an ice bath and oxalyl chloride (39 μl, 0.45 mmol) added with a microsyringe. A few drops of DMF were then added with a normal syringe. The mixture was allowed to warm to room temperature and stirring maintained for 5 h. The solvent was evaporated and the white compound that resulted dried under high vacuum for 1 h and used for the next step without any other purification. Diaza-18-crown-6-ether (39 mg, 0.15 mmol), freshly distilled THF (2 cm^3) and triethylamine (42 μL, 0.3 mmol) were placed in a two-necked flask under argon. The suspension was cooled to 0 °C by an ice bath and the acid chloride (0.3 mmol) in THF (2 cm^3) added slowly over 30 min. The mixture was allowed to warm to room temperature and stirring maintained overnight. The solution was filtered and the filtrate evaporated. The white solid obtained was purified by column chromatography (silica gel; CH_3OH : dichloromethane, 5 : 95). Yield: 70%. δ_H (400 MHz, $CDCl_3$, 25 °C, TMS): 7.79 (2 H, dd, $^3J = 8.6$, $^4J = 2$ Hz), 7.64 (2 H, d, $^4J = 2$ Hz), 7.46 (4 H, d, $^3J = 8.5$ Hz), 7.23 (4 H, d, $^3J = 8.5$ Hz), 6.92 (2 H, $^3J = 8.6$ Hz), 4.07 (8 H, m), 3.8 (8 H, m, large), 3.81–3.54 (24 H, m, large), 1.8 (8 H, m), 1.5 (8 H, m), 1.3 (20 H, large) and 0.87 (6 H, t). δ_C (100 MHz, $CDCl_3$, 25 °C, TMS): 171.8, 165.0, 154.3, 152.1, 149.0, 134.3, 121.5 (quat.), 128.4, 124.7, 122.2, 114.9, 112.2 (tert.), 71.1–70.8, 69.7, 69.4, 32.2, 30.1–29.9, 29.75–29.69, 29.5, 29.3, 26.35, 26.30, 23.0 (sec.) and 14.4 (prim.). IR: ν_{max} = 2918, 2850, 1724, 1628, 1596, 1466, 1427, 1272, 1193, 1132, 1074, 1019 and 753 cm^{-1}. UV-vis (25 °C, THF): $\lambda_{max}(\varepsilon)$ = 305 nm (sh, 16 × 10^3 M^{-1} cm^{-1}), 296 (19 × 10^3), 267 (37 × 10^3), 225 (58 × 10^3) and 207 (67 × 10^3). ES-MS ($CHCl_3$): m/z = 1448 (M^+, 90%) and 1225 (100%). Found: C, 72.81; H, 9.58; N, 1.92. **L1** · $0.2H_2O$ requires: C, 72.81; H, 9.61; N, 1.93%. M.p. = 101 °C.

***N,N′*-bis{4-[3,4-di(methoxy)benzoyloxy]benzyl}-1,10-diaza-4,7,13,16-tetraoxacyclooctadecane (L2).** Sodium carbonate (0.83 g, 7.83 mmol) and 1,10-diaza-4,7,13,16-tetraoxacyclooctadecane (0.934 g, 3.56 mmol) were stirred in acetonitrile (40 cm^3) for 1 h at 60 °C. A solution of **23** (2.5 g, 7.12 mmol) in acetonitrile (50 cm^3) was added and the mixture heated at 60 °C for 48 h. After removal of the solvent, the compound was extracted with dichloromethane (100 cm^3) and washed with water (3 × 100 cm^3). Ligand **L2** was precipitated from a mixture of acetonitrile/dichloromethane (3 : 7). Yield: 1.172 g (41%). δ_H (400 MHz, $CDCl_3$, 25 °C, TMS): 7.83 (2 H, dd, $^3J = 8$, $^4J = 2$ Hz), 7.66 (2 H, d, $^4J = 2$ Hz), 7.39 (4 H, d, $^4J = 9$ Hz), 7.12 (4 H, d, $^3J = 9$ Hz), 6.93 (2 H, d, $^3J = 8$ Hz), 3.96 (6 H, s), 3.95 (6 H, s), 3.71–3.60 (20 H, m) and 2.84 (8 H, t, $^3J = 6$ Hz). δ_C (100 MHz, $CDCl_3$, 25 °C, TMS): 165.0–137.3 (quat.), 129.7 (tert.), 124.3, 121.9, 121.4, 112.3, 110.3, 70.7 (sec.), 70.0, 59.4, 56.0 (prim.) and 53.8. IR: ν_{max} = 2879, 2800, 1720, 1598, 1588, 1512, 1418, 1189, 1086, 1013, 755 and 639 cm^{-1}. ESI-MS ($CHCl_3$): m/z = 803 (M^+) and 826 ([M + Na]$^+$). Found: C, 63.4; H, 6.6; N, 3.2. $C_{44}H_{54}N_2O_{12} \cdot 1.5H_2O$ requires: C, 63.7; H, 6.9; N, 3.4%. M.p. = 166 °C.

***N,N′*-bis{4-[3,4-di(decyloxy)benzoyloxy]benzyl}-1,10-diaza-4,7,13,16-tetraoxacyclo-octadecane (L3).** A solution of **24** (6.16 g, 10.2 mmol) in DMF (90 cm^3) was added to a solution of sodium carbonate (1.19 g, 11.22 mmol) and 1,10-diaza-4,7,13,16-tetraoxacyclooctadecane (1.34 g, 5.1 mmol) in DMF (40 cm^3). The mixture was heated at 100 °C for 24 h and the reaction allowed to cool to room temperature. After

addition of water (100 cm^3) the precipitate was filtered and washed with water and acetone to yield 5.74 g (86%) of **L3**. δ_H (400 MHz, $CDCl_3$, 25 °C, TMS): 7.80 (2 H, dd, $^3J = 8$, $^4J = 2$ Hz), 7.71 (2 H, d, $^4J = 2$ Hz), 7.45 (2 H, d, $^4J = 2$ Hz), 7.16 (4 H, d, $^3J = 8$ Hz), 7.05 (4 H, d, $^3J = 8$ Hz), 6.91 (2 H, d, $^3J = 8$ Hz), 4.06 (8 H, m), 3.70–3.60 (20 H, m), 2.84 (8 H, t, $^3J = 6$ Hz), 1.84 (4 H, m), 1.53–1.21 (56 H, m) and 0.88 (12 H, m). δ_C (100 MHz, $CDCl_3$, 25 °C, TMS): 165.1–137.2 (quat.), 129.7 (tert.), 124.3, 121.7, 121.4, 114.6, 112.0, 70.7–22.7 (sec.) and 14.1 (prim.). IR: ν_{max} = 2918, 2850, 1722, 1516, 1189, 1086 and 755. ESI-MS (CH_3OH): m/z = 1307.86 ($[M + H]^+$) and 654.87 ($[M + 2H]^{2+}$). Found: C, 73.3; H, 9.7; N, 2.1. $C_{80}H_{126}N_2O_{12}$ requires: C, 73.5; H, 9.7; N, 2.1%. M.p. = 85 °C.

***N,N′*-bis{4-[3,4-di(hexadecyloxy)benzoyloxy]benzyl}-1,10-diaza-4,7,13,16-tetraoxacyclo-octadecane (L4).** Prepared by a method similar to the one described for **L3**. Yield: 3.45 g (89%). δ_H (400 MHz, $CDCl_3$, 25 °C, TMS): 7.79 (2 H, dd, $^3J = 9$, $^4J = 2$ Hz), 7.65 (2 H, d, $^4J = 2$ Hz), 7.38 (4 H, d, $^3J = 8$ Hz), 7.11 (4 H, d, $^3J = 8$ Hz), 6.91 (2 H, d, $^3J = 9$ Hz), 4.06 (8 H, m), 3.70–3.60 (20 H, m), 2.84 (8 H, t, ^3J = 6 Hz), 1.84 (4 H, m), 1.53–1.21 (104 H, m) and 0.88 (12 H, m). δ_C (100 MHz, $CDCl_3$, 25 °C, TMS): 165.1–137.2 (quat.), 129.7 (tert.), 124.3, 122.4, 121.7, 114.6, 111.9, 70.7–22.7 (sec.) and 14.1 (prim.). ν_{max} = 2918, 2850, 1722, 1516, 1189, 1086 and 755. ESI-MS ($CDCl_3$): m/z = 1667.3 ($[M + Na]^+$) and 1645.2 ($[M + H]^+$). Found: C, 75.7; H, 10.8; N, 1.7. $C_{104}H_{174}N_2O_{12}$ requires: C, 76.0; H, 10.7; N, 1.7%. M.p. = 93 °C.

***N,N′*-bis{4-[3,4,5-tri(decyloxy)benzoyloxy]benzyl}-1,10-diaza-4,7,13,16-tetraoxacyclo-octadecane (L5).** Prepared by a method similar to the one described for **L3**. Yield: 41%. δ_H (400 MHz, $CDCl_3$, 25 °C, TMS): 7.41 (4 H, s), 7.40 (4 H, d, $J^3 = 8.4$ Hz), 7.13 (4 H, d, $J^3 = 8.4$ Hz), 4.05 (6 H, m), 3.72 (2 H, s), 3.64 (6 H, m), 2.85 (4 H, dd, $J^3 = 5.7$ Hz), 1.80 (6 H, m), 1.49 (6 H, m), 1.29 (38 H, large) and 0.88 (9 H, m). δ_C (100 MHz, $CDCl_3$, 25 °C, TMS): 165.2, 153.0, 150.0, 143.1, 137.4, 129.8, 124.1, 121.5, 108.7, 73.7, 70.8, 70.2, 69.4, 59.5, 53.9, 32.06, 32.03, 30.4, 29.85, 29.81, 29.80, 29.75, 29.72, 29.70, 29.54, 29.51, 29.47, 29.44, 26.21, 26.19, 22.82, 22.80 and 14.2. IR: ν_{max} = 2919, 2851, 1731, 1429, 1336, 1205, 1191, 1118, 961 and 749. UV-vis (25 °C, THF): $\lambda_{max}(\varepsilon)$ = 310 (sh, 4200), 274 (21 000) and 219 (66 000). ES-MS: m/z = 1621 (M^+, 85%) and 811 (M^{2+}, 93%). Found: C, 73.91; H, 10.35. **L5** · $0.25H_2O$ requires: C, 73.92; H, 10.33. M.p. = 37 °C.

Complexes. The general procedure used was as follows: A 10^{-2} M solution of the ligand in THF (dichloromethane for **L2** and **L5**) was added to a 10^{-2} M solution of the hydrated lanthanide (Ln = Eu, Tb) salt in THF (EtOH for $EuCl_3 \cdot nH_2O$; 10^{-1} M in MeCN for $Ln(NO_3)_3 \cdot nH_2O$). The mixture was stirred for 2 h (24 h in the case of the complexes with **L1** and **L5**) under an inert atmosphere and the solvent evaporated under a nitrogen flux, before recrystallization from acetonitrile (with the exception of complexes of **L1** and **L5**). Elemental analyses are reported in Table 1 while the thermogram of the Eu**L3** complex is given in Figure S4 of the ESI.†

X-ray crystallography

Data collection for **L2**§ was made on an Oxford Diffraction/Kuma diffractometer with kappa geometry and a CCD KM4/sapphire detector. Data reduction and determination of the unit cell parameters were undertaken using CrysAlis RED.[56] Structure solution and refinement were performed with SHELXTL release 5.1.[57]

Small angle diffraction X-ray scattering

The SAXS patterns were obtained using two different experimental setups. In all cases, a linear monochromatic Cu-Kα_1 beam (λ = 1.5405 Å) was obtained using a sealed-tube generator (900 W) equipped with a bent quartz monochromator. In the first setup, the transmission Guinier geometry was used, whereas a Debye–Scherrer-like geometry was used in the second experimental setup. In all cases, the crude powder was filled into Lindemann capillaries of 1 mm diameter. An initial set of diffraction patterns was recorded on an image plate. Periodicities up to 80 Å could be measured and the sample temperature controlled to within ±0.3 °C. The second set of diffraction patterns were recorded with a curved Inel CPS 120 counter gas-filled detector linked to a data acquisition computer. Here periodicities up to 60 Å could be measured and the sample temperature controlled to within ±0.05 °C. The feature occurring close to the beam stopper in Fig. 5 is not a reflection. It arises from interference with the edges of the beam stopper and is typically observed with lanthanide compounds which have a large absorption coefficient, resulting in a less intense fundamental reflection and therefore a poorer signal-to-noise ratio.

Acknowledgements

Financial support from the Swiss National Science Foundation, National Research Program 47 "Supramolecular Functional Materials" is gratefully acknowledged. We thank B. Hernach for the synthesis of **L3**, H. Lartigue for the TG/DTA measurements, J.-P. Rivera for his help with the POM experiments, F. Sepulveda and A. Dorcier for recording the MS spectra and F. Gumy for gathering some of the luminescence data.

References

1 K. Binnemans and C. Görller-Walrand, *Chem. Rev.*, 2002, **102**, 2303.
2 J. W. Emsley and J. C. Lindon, *NMR Spectroscopy Using Liquid Crystal Solvents*, Pergamon Press, New York, 1975.
3 M. A. Contreras, J. Ubach, O. Millet, J. Rizo and M. Pons, *J. Am. Chem. Soc.*, 1999, **121**, 8947.
4 L. Ozawa and M. Itoh, *Chem. Rev.*, 2003, **103**, 3835.
5 B. Donnio, D. Guillon, D. W. Bruce and R. Deschenaux, in *Comprehensive Coordination Chemistry II: From Biology to Nanotechnology*, ed. J. A. McCleverty, T. J. Meyer, M. Fujita and A. Powell, Elsevier, Oxford, 2003, ch. 79, pp. 357–627.
6 L. J. Yu and M. M. Labes, *Appl. Phys. Lett.*, 1977, **31**, 719.
7 C. Piechocki, J. Simon, J. J. André, D. Guillon, P. Petit, A. Skoulios and P. Weber, *Chem. Phys. Lett.*, 1985, **122**, 124.
8 Y. G. Galyametdinov, G. I. Ivanova and I. V. Ovchinnikov, *Bull. Acad. Sci. USSR Div. Chem. Sci. (Engl. Transl.)*, 1991, **40**, 1109.
9 Y. G. Galyametdinov, G. I. Ivanova, A. V. Prosvirin and O. Kadkin, *Russ. Chem. Bull.*, 1994, **43**, 938.
10 K. Binnemans, Y. G. Galyametdinov, S. R. Collinson and D. W. Bruce, *J. Mater. Chem.*, 1998, **8**, 1551.
11 H. Deng, D. L. Gin and R. C. Smith, *J. Am. Chem. Soc.*, 1998, **120**, 3522.
12 H. Nozary, C. Piguet, P. Tissot, G. Bernardinelli, J.-C. G. Bünzli, R. Deschenaux and D. Guillon, *J. Am. Chem. Soc.*, 1998, **120**, 12274.
13 E. Guillet, D. Imbert, R. Scopelliti and J.-C. G. Bünzli, *Chem. Mater.*, 2004, **16**, 4063.
14 K. Driesen and K. Binnemans, *Liq. Cryst.*, 2004, **31**, 601.
15 K. Binnemans, L. Jongen, C. Bromant, D. Hinz and G. Meyer, *Inorg. Chem.*, 2000, **39**, 5938.
16 L. Jongen, D. Hinz, G. Meyer and K. Binnemans, *Chem. Mater.*, 2001, **13**, 2243.
17 K. Binnemans, Y. G. Galyametdinov, R. Van Deun, D. W. Bruce, S. R. Collinson, A. P. Polishchuk, I. Bikchantaev, W. Haase, A. V. Prosvirin, L. Tinchurina, I. Litvinov, A. Gubajdullin, A. Rakhmatullin, K. Uytterhoeven and L. Van Meervelt, *J. Am. Chem. Soc.*, 2000, **122**, 4335.

18 Y. G. Galyametdinov, W. Haase, L. Malykhina, A. Prosvirin, I. Bikchantaev, A. Rakhmatullin and K. Binnemans, *Chem.–Eur. J.*, 2001, **7**, 99.
19 K. Binnemans and K. Lodewyckx, *Supramol. Chem.*, 2003, **15**, 485.
20 K. Binnemans, K. Lodewyckx, B. Donnio and D. Guillon, *Chem.–Eur. J.*, 2002, **8**, 1101.
21 E. Terazzi, J.-M. Benech, J.-P. Rivera, G. Bernardinelli, B. Donnio, D. Guillon and C. Piguet, *Dalton Trans.*, 2003, **769**.
22 Z. Belarbi, J. Sirlin, J. Simon and J. J. André, *J. Phys. Chem.*, 1989, **93**, 8105.
23 K. Kasuga, M. Tsutsui, R. C. Petterson, K. Tatsumi, N. Van Opdenbosch, G. Pepe and E. F. Meyer Jr., *J. Am. Chem. Soc.*, 1980, **102**, 4835.
24 K. Binnemans, J. Sleven, S. De Feyter, F. C. De Schryver, B. Donnio and D. Guillon, *Chem. Mater.*, 2003, **15**, 3930.
25 K. Ban, K. Nishizawa, K. Ohta, A. M. van der Craats, J. M. Warman, I. Yamamoto and H. Shirai, *J. Mater. Chem.*, 2001, **11**, 321.
26 M. H. Qi and G. F. Liu, *ChemPhysChem*, 2003, **4**, 605.
27 M. H. Qi and G. F. Liu, *J. Phys. Chem. B*, 2003, **107**, 7640.
28 H. Miwa, N. Kobayashi, K. Ban and K. Ohta, *Bull. Chem. Soc. Jpn.*, 1999, **72**, 2719.
29 T. Nakai, K. Ban, K. Ohta and M. Kimura, *J. Mater. Chem.*, 2002, **12**, 844.
30 K. Binnemans and B. Gundogan, *J. Rare Earths (China)*, 2002, **20**, 249.
31 D. Demus, J. W. Goodby, G. W. Gray, H. W. Spiess and V. Vill, *Handbook of Liquid Crystals*, Wiley-VCH, Weinheim, 1998.
32 J. W. Goodby, G. H. Mehl, I. M. Saez, R. P. Tuffin, G. Mackenzie, R. Auzely-Velty, T. Benvegnu and D. Plusquellec, *Chem. Commun.*, 1998, 2057.
33 V. S. Sastri, J.-C. G. Bünzli, V. R. Rao, G. V. S. Rayudu and J. R. Perumareddi, *Modern Aspects of Rare Earths and Complexes*, Elsevier, Amsterdam, 2003.
34 S. Suárez, O. Mamula, D. Imbert, C. Piguet and J.-C. G. Bünzli, *Chem. Commun.*, 2003, 1226.
35 S. Suárez, D. Imbert, F. Gumy, C. Piguet and J.-C. G. Bünzli, *Chem. Mater.*, 2004, **16**, 3257.
36 R. P. Tuffin, K. J. Toyne and J. W. Goodby, *J. Mater. Chem.*, 1996, **6**, 1271.
37 J.-C. G. Bünzli and D. Wessner, *Helv. Chim. Acta*, 1981, **64**, 582.
38 J.-C. G. Bünzli, in Complexes with ionophores, , *Handbook on the Physics and Chemistry of Rare Earths*, ed. K. A. Gschneidner Jr. and L. Eyring, Elsevier, Amsterdam, 1987, vol. **9**, ch. 60, pp. 321–294.
39 J.-C. G. Bünzli and A. Giorgetti, *J. Less-Common Met.*, 1985, **112**, 355.
40 S. Suárez, PhD thesis, EPFL, 2004.
41 F. J. Steemers, W. Verboom, D. N. Reinhoudt, E. B. Vandertol and J. W. Verhoeven, *J. Am. Chem. Soc.*, 1995, **117**, 9408.
42 J.-C. G. Bünzli, in *Spectroscopic Properties of Rare Earths in Optical Materials*, ed. G. K. Liu and B. Jacquier, Springer-Verlag, Berlin, 2005, vol. **83**, ch. 11, pp. 462–499.
43 H. Nozary, C. Piguet, J.-P. Rivera, P. Tissot, G. Bernardinelli, N. Vulliermet, J. Weber and J.-C. G. Bünzli, *Inorg. Chem.*, 2000, **39**, 5286.
44 F. Neve, M. Ghedini and O. Francescangeli, *Liq. Cryst.*, 1996, **21**, 625.
45 D. Guillon, *Struct. Bonding*, 1999, **95**, 41.
46 E. Terazzi, S. Torelli, G. Bernardinelli, J.-P. Rivera, J.-M. Benech, C. Bourgogne, B. Donnio, D. Guillon, D. Imbert, J.-C. G. Bünzli, A. Pinto, D. Jeannerat and C. Piguet, *J. Am. Chem. Soc.*, 2005, **127**, 888.
47 J.-C. G. Bünzli, G. A. Leonard, D. Plancherel and G. Chapuis, *Helv. Chim. Acta*, 1986, **69**, 288.
48 R. Rodriguez-Cortinas, F. Avecilla, C. Platas-Iglesias, D. Imbert, J.-C. G. Bünzli, A. de Blas and T. Rodriguez-Blas, *Inorg. Chem.*, 2002, **41**, 5336.
49 J.-C. G. Bünzli and F. Pilloud, *Inorg. Chem.*, 1989, **28**, 2638.
50 J.-C. G. Bünzli, E. Moret and J.-R. Yersin, *Helv. Chim. Acta*, 1978, **61**, 762.
51 G. Schwarzenbach, *Complexometric Titrations*, Chapman and Hall, London, 1957.
52 Y. Kita, M. Arisawa, M. Gyoten, M. Nakajima, R. Hamada, H. Tohma and T. Takada, *J. Org. Chem.*, 1998, **63**, 6625.
53 P. A. Heiney, M. R. Stetzer, O. Y. Mindyuk, E. DiMasi, A. R. McGhie, H. Liu and A. B. Smith, *J. Phys. Chem. B*, 1999, **103**, 6206.
54 H. Nozary, C. Piguet, J.-P. Rivera, P. Tissot, P.-Y. Morgantini, J. Weber, G. Bernardinelli, J.-C. G. Bünzli, R. Deschenaux, B. Donnio and D. Guillon, *Chem. Mater.*, 2002, **14**, 575.
55 K. Kasuga and H. Hatakeyama, *Cellul. Chem. Technol.*, 1984, **18**, 469.
56 *CrysAlis RED v. 1.7.0*, Oxford Diffraction Ltd., Abingdon, Oxfordshire, OX14 4RX, UK, 2003.
57 *SHELXTL release 5.1*, Bruker AXS Inc., Madison, Wisconsin 53719, USA, 1997.